STRUCTURAL CHEMISTRY

ISSN 2053-2296

Fe^{III} in a high-spin state in bis(5-bromosalicylaldehyde 4-ethylthiosemicarbazonato-κ^3O,N^1,S)ferrate(III) nitrate monohydrate, the first example of such a cationic Fe^{III} complex unit

Robyn E. Powell,[a,b] Martin R. Lees,[c] Graham J. Tizzard[d] and Petra J. van Koningsbruggen[a,b]*

[a]College of Engineering and Physical Sciences, School of Infrastructure and Sustainable Engineering, Department of Chemical Engineering and Applied Chemistry, Aston University, Aston Triangle, Birmingham, West Midlands, B4 7ET, UK, [b]Aston Institute of Materials Research, Aston University, Birmingham, B4 7ET, UK, [c]Department of Physics, University of Warwick, Coventry, CV4 7AL, UK, and [d]National Crystallography Service, Chemistry, University of Southampton, Southampton, SO17 1BJ, UK. *Correspondence e-mail: p.vankoningsbruggen@aston.ac.uk

Received 6 September 2021
Accepted 20 December 2021

Edited by D. R. Turner, University of Monash, Australia

Keywords: iron(III); carbazone; high spin; tautomerism; crystal structure; magnetic susceptibility.

CCDC reference: 2129820

Supporting information: this article has supporting information at journals.iucr.org/c

The synthesis and crystal structure (100 K) of the title compound, $[Fe(C_{10}H_{11}BrN_3OS)_2]NO_3{\cdot}H_2O$, is reported. The asymmetric unit consists of an octahedral $[Fe^{III}(HL)_2]^+$ cation, where HL^- is H-5-Br-thsa-Et or 5-bromosalicylaldehyde 4-ethylthiosemicarbazonate(1−) {systematic name: 4-bromo-2-[(4-ethylthiosemicarbazidoidene)methyl]phenolate}, a nitrate anion and a noncoordinated water molecule. Each HL^- ligand binds *via* the thione S, the imine N and the phenolate O atom, resulting in an $Fe^{III}S_2N_2O_2$ chromophore. The ligands are orientated in two perpendicular planes, with the O and S atoms in *cis* and the N atoms in *trans* positions. This $[Fe(HL)_2](anion){\cdot}H_2O$ compound contains the first known cationic Fe^{III} entity containing two salicylaldehyde thiosemicarbazone derivatives. The Fe^{III} ion is in the high-spin state at 100 K. In addition, a comparative IR spectroscopic study of the free ligand and the ferric complex is presented, demonstrating that such an analysis provides a quick identification of the degree of deprotonation and the coordination mode of the ligand in this class of metal compounds. The variable-temperature magnetic susceptibility measurements (5–320 K) are consistent with the presence of a high-spin Fe^{III} ion with a zero-field splitting D = 0.439 (1) cm^{-1}.

1. Introduction

The history of Fe^{III} spin-crossover compounds goes back to the 1930s when Cambi & Szegö observed temperature-dependent spin isomerism in iron(III) tris(dithiocarbamate) (Cambi & Szegö, 1931, 1933). Since then, two main families of Fe^{III} spin-crossover systems have been extensively studied: those containing ligands sporting chalcogen donor atoms and those based on multidentate *N*,*O*-donating Schiff base-type ligands (van Koningsbruggen *et al.*, 2004; Harding *et al.*, 2016); it has been found that the magnetic interconversion between the low-spin (S = 1/2) and high-spin (S = 5/2) state in Fe^{III} systems can be triggered by a change in temperature or pressure, or by light irradiation (Hayami *et al.*, 2000; van Koningsbruggen *et al.*, 2004; Hayami *et al.*, 2009; Harding *et al.*, 2016).

Due to their switchable magneto-optical properties, various applications in the fields of molecular electronics and sensing have been suggested for these bistable materials (Létard *et al.*, 2004; Gütlich *et al.*, 2004; Gütlich & Goodwin, 2004; van Koningsbruggen *et al.*, 2004; Takahashi *et al.*, 2006; Halcrow, 2013; Lefter *et al.*, 2016; Molnár *et al.*, 2018; Senthil Kumar *et*

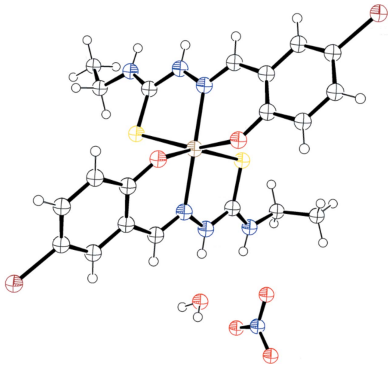

al., 2017; Rubio-Giménez *et al.*, 2019; Tissot *et al.*, 2019; Karuppannan *et al.*, 2021). Accordingly, in order to realise the full potential of spin-crossover materials in applications, the quest for knowledge is focused on how to use chemical synthesis in order to tune the spin-transition characteristics such that the compounds can fulfil these particular functions.

Studies carried out by several research groups have demonstrated that *R*-salicylaldehyde 4*R*′-thiosemicarbazones are very versatile ligand systems that enable the tuning of the spin state of the Fe^{III} ion (van Koningsbruggen *et al.*, 2004; Phonsri *et al.*, 2017; Powell *et al.*, 2014, 2015, 2020, 2022; Powell, 2016; Yemeli Tido, 2010; Zelentsov *et al.*, 1973; Ryabova *et al.*, 1978, 1981*a*,*b*, 1982; Floquet *et al.*, 2003, 2006, 2009; Li *et al.*, 2013, 2016). In spite of this versatility, in all instances the Fe^{III} isomer is identical in that the Fe^{III} ion is in a distorted $FeS_2N_2O_2$ octahedral environment formed by two *O*,*N*,*S*-tridentate ligands, which are geometrically arranged in such a way that the S and O atoms are located in *cis* positions, whereas the N atoms occupy *trans* positions, *i.e.* each tridentate ligand coordinates in an equatorial plane (van Koningsbruggen *et al.*, 2004; Phonsri *et al.*, 2017; Powell *et al.*, 2014, 2015, 2020, 2022; Powell, 2016; Yemeli Tido, 2010; Zelentsov *et al.*, 1973; Ryabova *et al.*, 1978, 1981*a*,*b*, 1982; Floquet *et al.*, 2003, 2006, 2009; Li *et al.*, 2013).

It has been demonstrated that the electronic state of an Fe^{III} ion surrounded by two such *O*,*N*,*S*-tridentate thiosemicarbazonate ligands depends on the substituents and degree of deprotonation of the *R*-salicylaldehyde 4*R*′-thiosemicarbazone ligands, whereas the identity of the counter-ion and the nature and degree of solvation afford further tuning of the Fe^{III} spin state (Powell *et al.*, 2014, 2015, 2020, 2022; Powell, 2016; Yemeli Tido, 2010). We made use of the fact that in solution, the free *R*-salicylaldehyde 4*R*′-thiosemicarbazone ligand (H_2L) exists in two tautomeric forms, *i.e.* the thione and thiol forms. Moreover, the ligand may also be present in its neutral, anionic or dianionic form. We established that the formation of a particular type of Fe^{III} complex unit, *i.e.* neutral, monocationic or monoanionic, can be achieved by tuning the degree of deprotonation of the ligand through pH variation of the reaction solution during the synthesis (Powell *et al.*, 2014, 2015, 2020, 2022; Powell, 2016; Yemeli Tido, 2010; Floquet *et al.*, 2009).

For this work, we used 5-bromosalicylaldehyde 4-ethylthiosemicarbazone (abbreviated as H_2-5-Br-thsa-Et), with the correct systematic name for the ligand being 4-bromo-2-[(4-ethylthiosemicarbazidoidene)methyl]phenol, whose two tautomeric forms, *i.e.* the thione and thiol forms, are shown in Scheme 1.

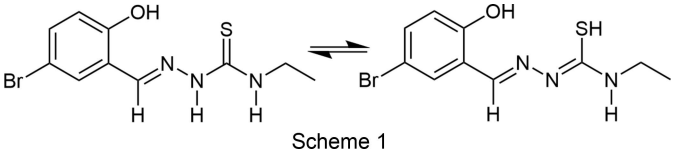

Scheme 1

Our present research enlarges the scope for tuning the structure and spin state of Fe^{III} compounds of *R*-salicylaldehyde 4*R*′-thiosemicarbazones, as we now report on [Fe(H-5-Br-thsa-Et)$_2$]NO_3·H_2O, (I) (Scheme 2), where H-5-Br-thsa-Et denotes 5-bromosalicylaldehyde 4-ethylthiosemicarbazonate(1−), which contains the first known cationic Fe^{III} complex entity containing two salicylaldehyde thiosemicarbazone derivatives. Its structure was determined at 100 K and confirmed that Fe^{III} is in the high-spin state. Furthermore, an IR spectroscopic characterization of the free ligand and ferric complex (I) is presented together with a variable-temperature magnetic susceptibility study.

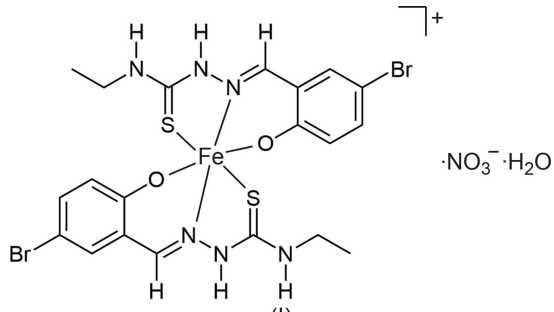

(I)

Scheme 2

2. Experimental

2.1. Spectroscopic and magnetic measurements

A room-temperature IR spectrum of 5-bromosalicylaldehyde 4-ethylthiosemicarbazone in the range 4000–400 cm^{-1} was recorded on a PerkinElmer FT–IR spectrometer Spectrum RXI using KBr pellets. IR spectroscopic measurements of (I) in the range 4000–600 cm^{-1} were carried out at room temperature using an ATR (attenuated total reflectance) PerkinElmer FT–IR Frontier spectrometer.

^1H and ^{13}C NMR spectra were recorded in DMSO-d_6 (DMSO is dimethyl sulfoxide) using a Bruker cryomagnet BZH 300/52 spectrometer (300 MHz) with the recorded chemical shifts in δ (in parts per million) relative to an internal standard of tetramethylsilane (TMS).

Measurements of direct current (dc) magnetic susceptibility, χ_M, *versus* temperature, *T*, were conducted in the temperature range 5–320 K, heating at a rate of 2 K min^{-1} in an applied field, $\mu_0 H$, of 0.1 T, using a Quantum Design MPMS-5S SQUID (Superconducting Quantum Interference Device) magnetometer. The SQUID magnetometer was calibrated using a standard palladium sample. The backgrounds due to the sample holder and the diamagnetic signal of the sample, estimated using Pascal's constants (Bain & Berry, 2008), were subtracted from the measured molar magnetic susceptibility χ_M.

2.2. Synthesis and crystallization

For the synthesis of 5-bromosalicylaldehyde 4-ethylthiosemicarbazone (H_2-5-Br-thsa-Et), 5-bromosalicylaldehyde (49 mmol, 9.85 g) was dissolved in ethanol (80 ml) with constant stirring and added to a solution of 4-ethyl-3-thiosemicarbazide (49 mmol, 5.84 g) in ethanol (40 ml). The corresponding mixture was refluxed for 120 min. The resulting solution was cooled to room temperature, the solid isolated by

Table 1
Experimental details.

Crystal data	
Chemical formula	$[Fe(C_{10}H_{11}BrN_3OS)_2]NO_3·H_2O$ [+solvent]
M_r	738.25
Crystal system, space group	Orthorhombic, *Pnna*
Temperature (K)	100
a, *b*, *c* (Å)	12.3595 (3), 23.2686 (6), 19.6406 (6)
V (Å^3)	5648.4 (3)
Z	8
Radiation type	Mo *Kα*
μ (mm^{-1})	3.56
Crystal size (mm)	0.19 × 0.01 × 0.01
Data collection	
Diffractometer	Rigaku FRE+ diffractometer equipped with HF Varimax confocal mirrors and an AFC12 goniometer and a HG Saturn 724+ detector
Absorption correction	Multi-scan (*CrysAlis PRO*; Rigaku OD, 2021)
T_{min}, T_{max}	0.740, 1.000
No. of measured, independent and observed [$I > 2\sigma(I)$] reflections	36848, 6477, 4297
R_{int}	0.088
(sin $\theta/\lambda)_{max}$ (Å^{-1})	0.649
Refinement	
$R[F^2 > 2\sigma(F^2)]$, $wR(F^2)$, *S*	0.057, 0.130, 1.02
No. of reflections	6477
No. of parameters	360
No. of restraints	6
H-atom treatment	H atoms treated by a mixture of independent and constrained refinement
$\Delta\rho_{max}$, $\Delta\rho_{min}$ (e Å^{-3})	0.68, −0.78

Computer programs: *CrystalClear-SM Expert* (Rigaku, 2013), *CrysAlis PRO* (Rigaku OD, 2021), *SHELXT2018* (Sheldrick, 2015*a*), *SHELXL2018* (Sheldrick, 2015*b*), *ORTEP-3 for Windows* (Farrugia, 2012) and *OLEX2* (Dolomanov *et al.*, 2009).

filtration, washed with ether and dried in a vacuum for 2 d (yield: 14.32 g, 47.55 mmol, 97.0%; m.p. 186 °C). H_2-5-Br-thsa-Et is soluble in methanol, acetone and DMSO. ^{1}H NMR (300 MHz, DMSO-d_6): δ (ppm) 11.42 (1H, *s*, OH), 10.28 (1H, *s*, S═C—NH), 8.32 (1H, *m*, N═CH), 8.66 [1H, *t*, S═C—NH(CH_2CH_3)], 6.80–7.38 (aromatic 3H, *m*, C—H), 3.60 (2H, *p*, NH—CH_2), 1.15 (3H, *t*, NHCH_2—CH_3). ^{13}C NMR (300 MHz, DMSO-d_6): δ (ppm) 176.5 (C═S), 155.5 (C—O), 137.0 (C═N), 133.2, 128.1, 122.9, 118.2 (C—C aromatic), 110.9 (C—Br), 38.2 (CH_2), 14.8 (CH_3). IR (cm^{-1}, KBr): 3299 (νOH), 3146 (νNH), 2990 (νCH_3), 2936 (νCH_2), 1613 (νC═N), 1601, 1550 (νC═C), 1237 (νC—N), 1047 (νC═S).

For the synthesis of $[Fe(H\text{-}5\text{-}Br\text{-}thsa\text{-}Et)_2]NO_3·H_2O$, (I), $Fe(NO_3)_3·9H_2O$ (1.0 mmol, 0.40 g) was dissolved in distilled water (5 ml). The ligand H_2-5-Br-thsa-Et (2.0 mmol, 0.60 g) was dissolved in an ethanol/methanol/water mixture (5:5:1 *v*/*v*/*v*) with the addition of dimethylamine (40 wt% in water; 10 mmol, 0.51 ml). To this mixture, the Fe^{III} salt solution was added dropwise with constant stirring. The resulting dark-green solution was stirred and heated to 120 °C for approximately 10 min. The solution was allowed to stand at room temperature until crystals formed. The dark-green microcrystals were isolated by filtration and dried (yield: 0.54 g, 0.73 mmol, 73.2%). IR (cm^{-1}, ATR): 3313, 3226 (νNH), 3047 (νCH_3), 2997 (νCH_2), 1601 (νC═N), 1582, 1542 (νC═C ring), 1294 (νC—O), 1312 (νN—N), 819 (νC—S), 867, 1352 (νNO).

2.3. Refinement

Crystal data, data collection and structure refinement details are summarized in Table 1. Atoms H10*B* and H10*A* of the water solvent molecule were located at idealized geometrical positions and refined using the riding model, with U_{iso}(H) = 1.5U_{eq}(O). The water molecule was then refined as a rigid group. H atoms bonded to N atoms (H12, H13, H21 and H22) were located in a difference map and refined riding on their parent atoms, with U_{iso}(H) = 1.2U_{eq}(N). All other H atoms were included in the refinement in calculated positions, riding on their parent atoms, with C—H = 0.95 Å and U_{iso}(H) = 1.2U_{eq}(C) for methine (—CH═), C—H = 0.99 Å and U_{iso}(H) = 1.2U_{eq}(C) for methylene (–CH_2–), and C—H = 0.98 Å and U_{iso}(H) = 1.5U_{eq}(C) for methyl (–CH_3) H atoms. Additional details towards the structure refinement of (I) are as follows: the *SMTBX* solvent-masking routine, as implemented within *OLEX2*, was used to mask residual electron density from unidentified solvent (Dolomanov *et al.*, 2009). A solvent mask was calculated and 116 electrons were found in four voids per unit cell, with a combined volume of 360 Å^3. This is consistent with the presence of 0.375EtOH, 0.125MeOH and 0.25H_2O per asymmetric unit, which accounts for 116 electrons per unit cell. These proportions are an estimate and not all of the solvents are necessarily present, so this estimate has not been included in the structural or moiety formulae.

3. Results and discussion

In solution, the free ligand 5-bromosalicylaldehyde 4-ethylthiosemicarbazone (H_2L) exists in two tautomeric forms, *i.e.* the thione and thiol forms, as illustrated in Scheme 1. Consequently, in Fe^{III} compounds, the ligand may be present as either of the possible tautomers, and may be neutral, anionic or dianionic. Referring to the thiol tautomer, neutral H_2L has H atoms located on the phenol O atom and the thiol S atom. The first deprotonation step involving the phenol group results in the formation of 5-bromosalicylaldehyde 4-ethylthiosemicarbazonate(1−) (abbreviated as HL^-). Subsequent deprotonation yields 5-bromosalicylaldehyde 4-ethylthiosemicarbazonate(2−) (abbreviated as L^{2-}).

The crystal structure of bis[5-bromosalicylaldehyde 4-ethylthiosemicarbazonato(1−)-κ^3O,N^1,S]ferrate(III) nitrate monohydrate, $[Fe(H\text{-}5\text{-}Br\text{-}thsa\text{-}Et)_2]NO_3·H_2O$, (I) (Fig. 1), was determined at 100 K. The present compound crystallizes in the orthorhombic space group *Pnna*. The asymmetric unit is comprised of the $[Fe(H\text{-}5\text{-}Br\text{-}thsa\text{-}Et)_2]^+$ cation, a nitrate anion and a water solvent molecule, and further ethanol, methanol and water in unknown proportions. To our knowledge, this is the first structure to be reported of a cationic Fe^{III} complex entity containing two salicylaldehyde thiosemicarbazone derivatives. Selected geometric parameters are given in Table 2. The Fe^{III} cation is coordinated by two singly depro-

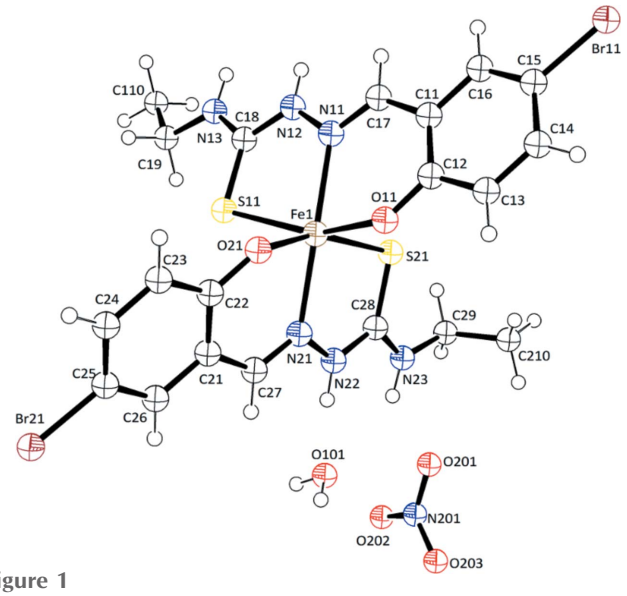

Figure 1
Projection showing the molecular structure and atom-numbering scheme for (I). Displacement ellipsoids are drawn at the 50% probability level.

tonated thione *O*,*N*,*S*-tridentate ligands. The 5-bromosalicylaldehyde 4-ethylthiosemicarbazonate(1−) ligands are deprotonated at the phenolate O atoms.

The $Fe^{III}O_2N_2S_2$ unit displays a distorted octahedral geometry, as corroborated by the bond angles involving the ligand donor atoms and the Fe1 atom.

The Fe1 donor atom distances involving the two tridentate anionic H-5-Br-thsa-Et ligands are Fe1—S11 = 2.4404 (15) Å, Fe1—S21 = 2.4615 (14) Å, Fe1—O11 = 1.952 (3) Å, Fe1—O21 = 1.944 (3) Å, Fe1—N11 = 2.176 (4) Å and Fe1—N21 = 2.161 (4) Å for the bond distances from Fe^{III} to the thione S, phenolate O and imine N atoms of the two crystallographically independent ligands. The Fe–donor atom bond distances suggest that the Fe^{III} cation in the present compound is in the high-spin state at 100 K. In fact, these bond distances compare rather well to these involving high-spin Fe^{III} in $[(CH_3)_2NH_2]$-[Fe(3-OEt-thsa)$_2$] [3-OEt-thsa is 3-ethoxysalicylaldehyde thiosemicarbazonato(2−)] determined at 100 K, *i.e.* Fe1—S1 = 2.4320 (6) Å, Fe1—S101 = 2.4389 (7) Å, Fe1—O1 = 1.9806 (16) Å, Fe1—O101 = 1.9595 (16) Å, Fe1—N1 = 2.167 (2) Å and Fe1—N101 = 2.131 (2) Å for the bond distances from Fe^{III} to the thiol S, phenolate O and imine N atoms of the two crystallographically independent ligands (Powell *et al.*, 2022). In fact, the typical distances for Fe—S, Fe—O and Fe—N bonds are 2.23–2.31, 1.93–1.95 and 1.88–1.96 Å, respectively, for low-spin Fe^{III} in compounds of formula [cation(1+)][Fe{*R*-salicylaldehyde 4*R*′-thiosemicarbazonato(2−)}$_2$]·*x*(solvent), and 2.40–2.44, 1.96–1.99 and 2.05–2.15 Å, respectively, for the corresponding high-spin Fe^{III} compounds (van Koningsbruggen *et al.*, 2004), albeit that the Fe^{III}—S distance involves the thiol moiety rather than the thione entity that is present in title compound (I). Variable-temperature magnetic susceptibility measurements (5–300 K) confirm that the Fe^{III} ion in this compound is indeed in the high-spin state over the stated temperature range (*vide infra*) (Powell, 2016).

Table 2
Selected geometric parameters (Å, °).

Fe1—S11	2.4404 (15)	Fe1—O21	1.944 (3)
Fe1—S21	2.4615 (14)	Fe1—N11	2.176 (4)
Fe1—O11	1.952 (3)	Fe1—N21	2.161 (4)
S11—Fe1—S21	98.70 (5)	C28—S21—Fe1	99.60 (17)
O11—Fe1—S11	158.16 (11)	C12—O11—Fe1	134.9 (3)
O11—Fe1—S21	92.89 (11)	C22—O21—Fe1	134.2 (3)
O11—Fe1—N11	83.71 (14)	C17—N11—Fe1	126.8 (3)
O11—Fe1—N21	112.13 (14)	C18—N12—N11	120.4 (4)
O21—Fe1—S11	90.03 (11)	C27—N21—Fe1	126.3 (3)
O21—Fe1—S21	160.48 (11)	C28—N22—N21	121.2 (4)
O21—Fe1—O11	84.89 (15)	C12—C11—C17	124.1 (5)
O21—Fe1—N11	114.03 (15)	O11—C12—C11	123.0 (5)
O21—Fe1—N21	83.82 (14)	N11—C17—C11	124.9 (5)
N11—Fe1—S11	79.00 (11)	N12—C18—S11	121.3 (4)
N11—Fe1—S21	84.89 (11)	C22—C21—C27	123.5 (4)
N21—Fe1—S11	88.32 (11)	O21—C22—C21	121.5 (4)
N21—Fe1—S21	79.05 (11)	N21—C27—C21	125.6 (4)
N21—Fe1—N11	157.80 (15)	N22—C28—S21	120.9 (4)
C18—S11—Fe1	99.81 (17)		

The tridentate ligands in (I) coordinate to the Fe^{III} cation to give an $Fe^{III}O_2N_2S_2$ octahedral environment, forming six- and five-membered chelate rings. The values of the r.m.s. deviations from the least-squares planes of the atoms comprising the five-membered chelate rings (Fe1/N11/N12/C18/S11 and Fe1/N21/N22/C28/S21) are 0.071 and 0.007 Å, respectively; the corresponding values for the six-membered chelate rings (Fe1/N11/C17/C11/C12/O11 and Fe1/N21/C27/C21/C22/O21) are 0.073 and 0.102 Å, respectively. These geometric features are associated with O11—Fe1—N11 and O21—Fe1—N21 bite angles of 83.71 (14) and 83.82 (14)°, respectively; as expected, the bite angles of the six-membered chelate ring are larger than those of the five-membered chelate ring [S11—Fe1—N11 = 79.00 (11)° and S21—Fe1—N21 = 79.05 (11)°]. The

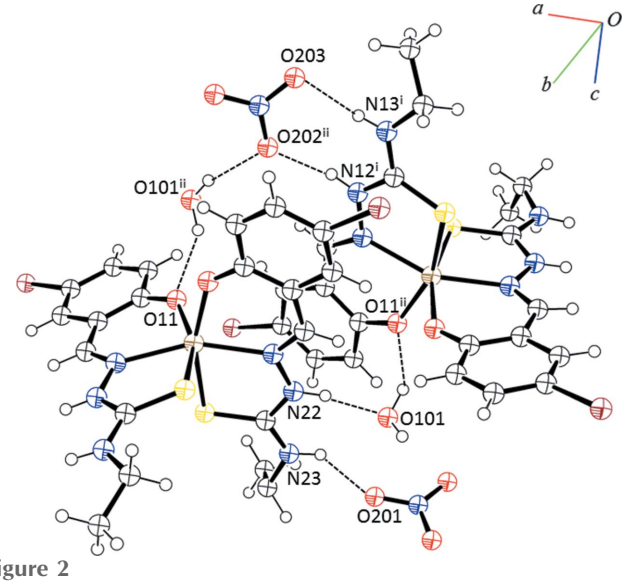

Figure 2
Projection showing the hydrogen-bonding interactions of (I). Displacement ellipsoids are drawn at the 50% probability level. Dashed lines indicate hydrogen bonds. [Symmetry codes: (i) $x+1, -y+\frac{1}{2}, -z+\frac{3}{2}$; (ii) $x-\frac{1}{2}, y, -z+1$; (iii) $x, -y+\frac{1}{2}, -z+\frac{3}{2}$.]

conformations of the five- and six-membered chelate rings of (I) are such that there is no major puckering.

5-Bromosalicylaldehyde 4-ethylthiosemicarbazone appears to be in its thione form, *i.e.* it is deprotonated at the phenolate O atoms (O11 and O21) and possesses a H atom on the hydrazinic N atoms (N12 and N22). The protonation of the hydrazinic N atoms (N12 and N22) confirms the presence of the thione form of the tautomer, which is corroborated by the C═S bond distances of the 5-bromosalicylaldehyde 4-ethylthiosemicarbazonate(1−) ligands being closer to those having a C═S bond order of two. The C—S bond distances are C18—S11 = 1.692 (5) Å and C28—S21 = 1.698 (5) Å. Furthermore, electron delocalization over the five-membered chelate ring involving each ligand is inferred from the values for the N—N and C—N bond distances of each ligand that is coordinated to the Fe^{III} cation. These bond distances are indicative of a bond order greater than one, *i.e.* the N11—N12 and N21—N22 bond distances are 1.396 (6) and 1.376 (5) Å, respectively, and the N12—C18 and N22—C28 bond distances are 1.349 (6) and 1.352 (6) Å, respectively.

The hydrogen-bonding interactions of (I) are listed in Table 3 and displayed in Fig. 2. The nitrate anion is involved in hydrogen-bonding interactions with the 5-bromosalicylaldehyde 4-ethylthiosemicarbazonate(1−) ligand. These hydrogen-bonding interactions include terminal atoms N13 and N23 of the ligand forming contacts with nitrate O atoms, O203 and $O201^{iv}$ [symmetry code: (iv) $x-1, -y+\frac{3}{2}, -z+\frac{3}{2}$], respectively. Atom N12 of the ligand forms an N12—H12···O202 contact with nitrate atom O202. Also, the nitrate anion forms a hydrogen-bonding interaction with water atom $O101^{ii}$ [symmetry code: (ii) $x-\frac{1}{2}, y, -z+1$]. Therefore, the nitrate anion is involved in two hydrogen-bonding ring systems which connect the Fe^{III} units. The first ring system is formed between two Fe^{III} units, two water solvent molecules and a nitrate anion. The ring system is formed by the following contacts N12—H12···O202, O101—H10*A*···$O202^{ii}$, O101—H10*B*···O11 and N22—H22···$O101^{ii}$, giving rise to an $R_4^5(18)$ ring system. Furthermore, the second ring system is created by the contacts N12—H12···O202 and N13—H13···O203, giving rise to an $R_2^2(8)$ ring system. The structure does include a halogen–chalcogen contact [Br21···$S11^{v}$ = 3.5103 (13) Å; symmetry code: (v) $-x+1, -y+1, -z+1$] and a halogen–halogen contact [Br11···$Br11^{vi}$ = 3.5999 (11) Å; symmetry code: (vi) $-x+\frac{5}{2}, -y+2, z$] which is less than the sum of the van der Waal radii.

Table 3
Hydrogen-bond geometry (Å, °).

D—H···*A*	*D*—H	H···*A*	*D*···*A*	*D*—H···*A*
N12—H12···O202	0.87 (3)	1.92 (4)	2.733 (6)	155 (5)
N13—H13···O203	0.88 (3)	2.02 (3)	2.890 (6)	176 (5)
N22—H22···$O101^{ii}$	0.87 (3)	1.85 (3)	2.695 (6)	166 (5)
N23—H23···$O201^{iv}$	0.87 (3)	2.23 (4)	2.887 (6)	133 (4)
O101—H10*A*···$O202^{ii}$	0.85	1.90	2.692 (6)	155
O101—H10*B*···O11	0.85	2.28	2.809 (6)	121

Symmetry codes: (ii) $x-\frac{1}{2}, y, -z+1$; (iv) $x-1, -y+\frac{3}{2}, -z+\frac{3}{2}$.

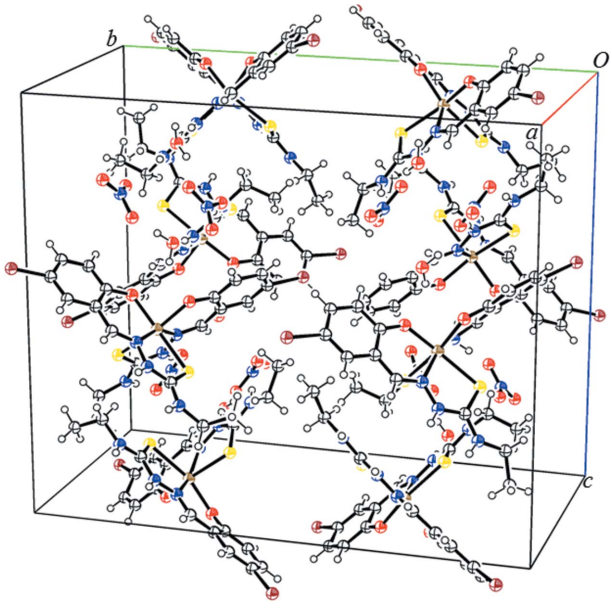

Figure 3
Projection showing the unit cell of (I). Displacement ellipsoids are drawn at the 50% probability level.

The assembly of the Fe^{III} units of the present compound is displayed in Fig. 3. The presence of both the NO_3^- anion and the water solvent molecule codetermines how the Fe^{III} units are packed in the crystal lattice. Complex salt (I) displays Fe^{III}···$Fe^{III}(x+\frac{1}{2}, y, -z+1)$ separations of 6.7661 (7) Å and Fe^{III}···$Fe^{III}(x, -y+\frac{1}{2}, -z+\frac{3}{2})$ separations of 7.2104 (16) Å. Despite the presence of the water solvent molecule and the nitrate anion, the Fe^{III} units are packed relatively close together within the crystal lattice. This feature could be due to the hydrogen-bonding ring systems (*vide supra*), which link the Fe^{III} units together *via* the hydrogen-bonding interactions of the water solvent molecule and the nitrate anion.

An IR spectroscopic characterization of the free ligand has been carried out, as well as a comparison with the IR spectrum of the ferric complex in order to assess the degree of deprotonation and the coordination mode of the ligand.

The IR spectrum of the free ligand, 5-bromosalicylaldehyde 4-ethylthiosemicarbazone (H_2-5-Br-thsa-Et), exhibits a strong band at 1613 cm^{-1}, which is assigned to the imine group that has been formed during the ligand synthesis, which involves the condensation of the salicylaldehyde moiety and the thiosemicarbazone moiety. Furthermore, the IR spectrum of the ligand exhibits a medium band at 3146 cm^{-1}, which is assigned to the νN—H vibration. The presence of the νN—H band in the spectrum of (I) evidences that the thione form of the ligand is coordinated to the central Fe^{III} cation. Upon coordination of the imine N atom, the νC═N band shifts from 1613 cm^{-1} in the free ligand to 1600 cm^{-1} in the complex. The νN—N band of the thiosemicarbazone moiety of the free ligand is found at 1105 cm^{-1}; the wavenumber increases to 1312 cm^{-1} for the νN—N band in the ferric complex. In comparison to the free ligand, the ferric complex does not show the presence of the νO—H vibration; this is due to the phenolic O atom having been deprotonated in order for the *O*,*N*,*S*-tridentate chelating ligand to coordinate the Fe^{III} atom

in the $[Fe(H\text{-}5\text{-}Br\text{-}thsa\text{-}Et)_2]^+$ cation. The corresponding νO—H band for the free ligand is found at 3299 cm^{-1}. The Fe^{III} cation is also coordinated to the S atom of the thiosemicarbazone moiety of the ligand. The νC═S band of the ligand that is coordinated to the Fe^{III} ion is assigned at 819 cm^{-1} in the ferric complex, but it is at a larger wavenumber in the free ligand, *i.e.* νC═S at 1046 cm^{-1}. The decrease in the frequency of the νC═S band in the thiosemicarbazone upon complexation of the ligand indicates coordination of the thione S atom to the Fe^{III} cation. The results of our analysis will be instrumental for the quick identification of the degree of deprotonation and the coordination mode of the ligand in other metal compounds as it is based on easily accessible IR spectroscopic measurements.

In the IR spectrum of the ferric complex, there are two bands which represent the presence of the nitrate anion within the crystal lattice; the νN—O bands of the NO_3^- anion are assigned at 866 and 1352 cm^{-1}, respectively. Furthermore, as evidenced from the crystallographic study of complex (I), there is hydrogen bonding within the crystal lattice; this is supported by the broad peaks observed for the νN—H bands assigned to the azomethine and terminal N atoms of the thiosemicarbazone moiety of the coordinated ligand.

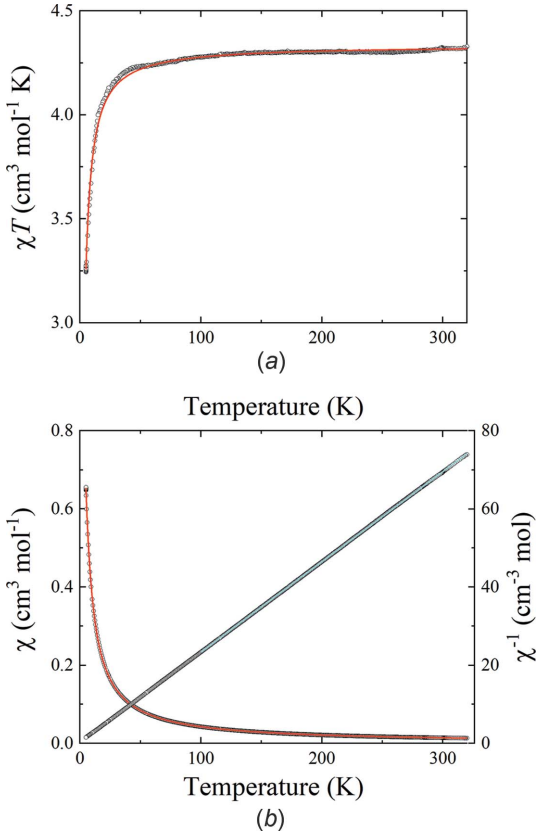

Figure 4
(*a*) $\chi_M T$ *versus* T for (I). The data were measured while heating at a rate of 2 K min^{-1} in an applied field $\mu_0 H$ of 0.1 T. (*b*) Temperature dependence of the corresponding molar magnetic susceptibility, χ_M, for (I). The solid red lines show fits to the data using Equation (1), with D = 0.439 (1) cm^{-1} and g = 2.0. The blue line in part (*b*) shows a fit of $\chi_M^{-1}(T)$ above 100 K using the Curie–Weiss law.

Variable-temperature magnetic susceptibility measurements (5–320 K) were carried out in order to confirm the spin state of the Fe^{III} ion. The temperature dependence of $\chi_M T$ for (I) is displayed in Fig. 4(*a*). $\chi_M T$ varies from 3.27 cm^3 mol^{-1} K at 5 K to an almost constant value of 4.33 (1) cm^3 mol^{-1} K [5.89 (1) μ_B/Fe] at higher temperatures (50–320 K). This is close to the expected value of 4.37 cm^3 mol^{-1} K (5.92 μ_B/Fe) for Fe^{III} in its high-spin state (S = 5/2), with an electronic g factor of 2.0023. A Curie–Weiss behaviour at high temperature is confirmed by the linear behaviour of $\chi_M^{-1}(T)$, and the fit to the Curie–Weiss law shown in Fig. 4(*b*) between 100 and 320 K gives a Weiss temperature of −0.5 (1) K and an effective moment of 5.86 (1) μ_B/Fe.

$\chi_M T$ drops rapidly below 20 K, reflecting a significant zero-field splitting of the S = 5/2 state. The spin Hamiltonian can be written as

$$H_S = H_{CEF} + H_z.$$

The crystalline electric field term

$$H_{CEF} = D\left[S_z^2 - S(S+1)/3\right] + E\left(S_x^2 - S_y^2\right),$$

where D and E are the axial and rhombic zero-field splitting, respectively. The ^6S high-spin state is split into three Kramers doublets, with the higher levels separated by $2D$ and $6D$ from the lowest energy level. The Zeeman energy $H_z = g\mu_B H S_x$ and then the molar magnetic susceptibility for E = 0 is

$$\chi_M = \frac{N_A g^2 \mu_B^2}{4k_B T}\left[\frac{1 + 9e^{-2X} + 25e^{-6X}}{1 + e^{-2X} + e^{-6X}}\right], \qquad (1)$$

where $X = D/k_B T$, N_A is Avogadro's number and k_B is the Boltzmann constant. A least-squares fit gives D = 0.439 (1) cm^{-1} with g = 2.0. This is in the range expected for high-spin Fe^{III} (Chen *et al.*, 2002; Yemeli Tido *et al.*, 2007). Fits with a finite E expected for a system with a rhombic distortion are possible, *cf.* Chen *et al.* (2002), but these require a knowledge of the ratio $\lambda = E/D$ from other studies, *e.g.* electron paramagnetic resonance spectroscopy or inelastic neutron scattering, and lower-temperature magnetic susceptibility data.

We thus reported the first structural characterization of a member of the family of $[Fe(HL^-)_2][anion(1-)]\cdot n(solvent)$ (H_2L = *R*-salicylaldehyde 4*R*′-thiosemicarbazone) compounds, which contains a cationic Fe^{III} entity. This further demonstrated the versatility in charge distribution that can be achieved using this ligand system, as neutral Fe^{III} complex units have been observed previously for $[Fe(HL^-)(L^{2-})]\cdot n(solvent)$, whereas anionic Fe^{III} units have been found to be present in $[cation(1+)][Fe(L^{2-})_2]\cdot n(solvent)$ (van Koningsbruggen *et al.*, 2004; Phonsri *et al.*, 2017; Powell *et al.*, 2014, 2015, 2020, 2022; Powell, 2016; Yemeli Tido, 2010; Zelentsov *et al.*, 1973; Ryabova *et al.*, 1978, 1981*a*,*b*, 1982; Floquet *et al.*, 2003, 2006, 2009; Li *et al.*, 2013).

The Fe^{III} ion is the high-spin state throughout the temperature range (5–320 K) over which the magnetic susceptibility data were recorded. Since this compound is the first example of a cationic Fe^{III} entity in this family, it is too early to attempt to relate the structural and electronic features of the material to the nature of the Fe^{III} spin state and to comment on the

reasons for the absence of Fe^{III} spin crossover. This as yet limited knowledge related to the present material is not unexpected as for the relatively well-known family of [cation(1+)][Fe(L^{2-})$_2$] compounds of which several members have been structurally and magnetically characterized (van Koningsbruggen *et al.*, 2004; Phonsri *et al.*, 2017; Powell *et al.*, 2014, 2015, 2020, 2022; Powell, 2016; Yemeli Tido, 2010; Zelentsov *et al.*, 1973; Ryabova *et al.*, 1978, 1981*a*,*b*, 1982; Floquet *et al.*, 2003, 2006, 2009; Li *et al.*, 2013, 2016), a correlation between structure and Fe^{III} spin state, including the occurrence of spin-crossover behaviour, has not yet been established. The reasons for this incomplete understanding lie in the occurrence of a spin-transition being governed by subtle structural and electronic modifications that are also tuned by the crystal packing, which in concert determine the ligand field strength and hence the manifestation of spin-crossover behaviour. These modifications depend on the nature of the ligands, the noncoordinating cation, the solvent molecules (if any) and the crystal packing. Clearly, the stabilization of Fe^{III} in a particular spin state is governed by a subtle balance of electronic and geometric parameters, as is implied by the fact that (NH_4)[Fe(5-Br-thsa)$_2$] (Ryabova *et al.*, 1981*b*) exists in slightly different polymorphs each with its distinct magnetic behaviour.

Our further research will focus on investigating the modulation of the Fe^{III} spin state upon varying the *R* and *R*′ substituents of the ligand, the noncoordinating anion, the degree of solvation and intermolecular interactions in such [Fe(HL^{-})$_2$][anion(1−)]·*n*(solvent) (H_2L = *R*-salicylaldehyde 4*R*′-thiosemicarbazone) compounds with the objective of defining the parameters for generating spin-crossover behaviour in these systems.

Acknowledgements

We thank the EPSRC UK National Crystallography Service (Coles & Gale, 2012) at the University of Southampton for the collection of the crystallographic data.

References

Bain, G. A. & Berry, J. F. (2008). *J. Chem. Educ.* **85**, 532–536.
Cambi, L. & Szegö, L. (1931). *Berichte*, **64**, 2591–2598.
Cambi, L. & Szegö, L. (1933). *Berichte*, **66**, 656–661.
Chen, C.-H., Lee, Y.-Y., Liau, B.-C., Elango, S., Chen, J.-H., Hsieh, H.-Y., Liao, F.-L., Wang, S.-L. & Hwang, L.-P. (2002). *J. Chem. Soc. Dalton Trans.* pp. 3001–3006.
Coles, S. J. & Gale, P. A. (2012). *Chem. Sci.* **3**, 683–689.
Dolomanov, O. V., Bourhis, L. J., Gildea, R. J., Howard, J. A. K. & Puschmann, H. (2009). *J. Appl. Cryst.* **42**, 339–341.
Farrugia, L. J. (2012). *J. Appl. Cryst.* **45**, 849–854.
Floquet, S., Boillot, M. L., Rivière, E., Varret, F., Boukheddaden, K., Morineau, D. & Négrier, P. (2003). *New J. Chem.* **27**, 341–348.
Floquet, S., Guillou, N., Négrier, P., Rivière, E. & Boillot, M. L. (2006). *New J. Chem.* **30**, 1621–1627.
Floquet, S., Muñoz, M. C., Guillot, R., Rivière, E., Blain, G., Réal, J. A. & Boillot, M. L. (2009). *Inorg. Chim. Acta*, **362**, 56–64.
Gütlich, P. & Goodwin, H. A. (2004). *Top. Curr. Chem.* **233**, 1–47.
Gütlich, P., van Koningsbruggen, P. J. & Renz, F. (2004). *Struct. Bonding*, **107**, 27–75.
Halcrow, M. A. (2013). Editor. *Spin-Crossover Materials*. Oxford: John Wiley & Sons Ltd.
Harding, D. J., Harding, P. & Phonsri, W. (2016). *Coord. Chem. Rev.* **313**, 38–61.
Hayami, S., Gu, Z., Shiro, M., Einaga, Y., Fujishima, A. & Sato, O. (2000). *J. Am. Chem. Soc.* **122**, 7126–7127.
Hayami, S., Hiki, K., Kawahara, T., Maeda, Y., Urakami, D., Inoue, K., Ohama, M., Kawata, S. & Sato, O. (2009). *Chem. Eur. J.* **15**, 3497–3508.
Karuppannan, S. K., Martín-Rodríguez, A., Ruiz, E., Harding, P., Harding, D. J., Yu, X., Tadich, A., Cowie, B., Qi, D. & Nijhuis, C. A. (2021). *Chem. Sci.* **12**, 2381–2388.
Koningsbruggen, P. J. van, Maeda, Y. & Oshio, H. (2004). *Top. Curr. Chem.* **233**, 259–324.
Lefter, C., Davesne, V., Salmon, L., Molnár, G., Demont, P., Rotaru, A. & Bousseksou, A. (2016). *Magnetochemistry*, **2**, 18.
Létard, J. F., Guionneau, P. & Goux-Capes, L. (2004). *Top. Curr. Chem.* **235**, 221–249.
Li, Z. Y., Dai, J. W., Shiota, Y., Yoshizawa, K., Kanegawa, S. & Sato, O. (2013). *Chem. Eur. J.* **19**, 12948–12952.
Li, Z.-Y., Ohtsu, H., Kojima, T., Dai, J.-W., Yoshida, T., Breedlove, B. K., Zhang, W.-X., Iguchi, H., Sato, O., Kawano, M. & Yamashita, M. (2016). *Angew. Chem. Int. Ed.* **55**, 5184–5189.
Molnár, G., Rat, S., Salmon, L., Nicolazzi, W. & Bousseksou, A. (2018). *Adv. Mater.* **30**, 1703862.
Phonsri, W., Darveniza, L. C., Batten, S. R. & Murray, K. S. (2017). *Inorganics*, **5**, 51.
Powell, R. E. (2016). PhD Thesis, Aston University, Birmingham, UK.
Powell, R. E., Schwalbe, C. H., Tizzard, G. J. & van Koningsbruggen, P. J. (2014). *Acta Cryst.* C**70**, 595–598.
Powell, R. E., Schwalbe, C. H., Tizzard, G. J. & van Koningsbruggen, P. J. (2015). *Acta Cryst.* C**71**, 169–174.
Powell, R. E., Stöger, B., Knoll, C., Müller, D., Weinberger, P. & van Koningsbruggen, P. J. (2020). *Acta Cryst.* C**76**, 625–631.
Powell, R. E. C. H., Lees, M. R., Tizzard, G. J. & van Koningsbruggen, P. J. (2022). *Acta Cryst.* C**78**. In preparation.
Rigaku (2013). *CrystalClear-SM Expert*. Riguku Corporation, The Woodlands, Texas, USA.
Rigaku OD (2021). *CrysAlis PRO*. Rigaku Oxford Diffraction, Wrocłow, Poland.
Rubio-Giménez, V., Bartual-Murgui, C., Galbiati, M., Núñez-López, A., Castells-Gil, J., Quinard, B., Seneor, P., Otero, E., Ohresser, P., Cantarero, A., Coronado, E., Real, J. A., Mattana, R., Tatay, S. & Martí-Gastaldo, C. (2019). *Chem. Sci.* **10**, 4038–4047.
Ryabova, N. A., Ponomarev, V. I., Atovmyan, L. O., Zelentsov, V. V. & Shipilov, V. I. (1978). *Koord. Khim.* **4**, 119–126.
Ryabova, N. A., Ponomarev, V. I., Zelentsov, V. V. & Atovmyan, L. O. (1981*a*). *Kristallografiya*, **26**, 101–108.
Ryabova, N. A., Ponomarev, V. I., Zelentsov, V. V. & Atovmyan, L. O. (1982). *Kristallografiya*, **27**, 81–91.
Ryabova, N. A., Ponomarev, V. I., Zelentsov, V. V., Shipilov, V. I. & Atovmyan, L. O. (1981*b*). *J. Struct. Chem.* **22**, 234–238.
Senthil Kumar, K. & Ruben, M. (2017). *Coord. Chem. Rev.* **346**, 176–205.
Sheldrick, G. M. (2015*a*). *Acta Cryst.* A**71**, 3–8.
Sheldrick, G. M. (2015*b*). *Acta Cryst.* C**71**, 3–8.
Takahashi, K., Cui, H.-B., Okano, Y., Kobayashi, H., Einaga, Y. & Sato, O. (2006). *Inorg. Chem.* **45**, 5739–5741.
Tissot, A., Kesse, X., Giannopoulou, S., Stenger, I., Binet, L., Rivière, E. & Serre, C. (2019). *Chem. Commun.* **55**, 194–197.
Yemeli Tido, E. W. (2010). PhD Thesis, University of Groningen, The Netherlands.
Yemeli Tido, E. W., Vertelman, E. J. M., Meetsma, A. & van Koningsbruggen, P. J. (2007). *Inorg. Chim. Acta*, **360**, 3896–3902.
Zelentsov, V. V., Bogdanova, L. G., Ablov, A. V., Gerbeleu, N. V. & Dyatlova, C. V. (1973). *Russ. J. Inorg. Chem.* **18**, 2654–2657.

supporting information

Acta Cryst. (2022). C**78**, 63-69 [https://doi.org/10.1107/S2053229621013462]

Fe^{III} in a high-spin state in bis(5-bromosalicylaldehyde 4-ethylthiosemicarbazonato-κ^3O,N^1,S)ferrate(III) nitrate monohydrate, the first example of such a cationic Fe^{III} complex unit

Robyn E. Powell, Martin R. Lees, Graham J. Tizzard and Petra J. van Koningsbruggen

Computing details

Data collection: *CrystalClear*-SM Expert (Rigaku, 2013); cell refinement: *CrysAlis PRO* (Rigaku OD, 2021); data reduction: *CrysAlis PRO* (Rigaku OD, 2021); program(s) used to solve structure: SHELXT2018 (Sheldrick, 2015a); program(s) used to refine structure: *SHELXL2018* (Sheldrick, 2015b); molecular graphics: OLEX2 (Dolomanov *et al.*, 2009) and *ORTEP-3 for Windows* (Farrugia, 2012); software used to prepare material for publication: OLEX2 (Dolomanov *et al.*, 2009).

Bis[4-bromo-2-({[(ethylcarbamothioyl)amino]imino}methyl)phenolato-κ^3O,N^1,S]ferrate(III) nitrate monohydrate

Crystal data

$[Fe(C_{10}H_{11}BrN_3OS)_2]NO_3{\cdot}H_2O$[+solvent]
M_r = 738.25
Orthorhombic, *Pnna*
a = 12.3595 (3) Å
b = 23.2686 (6) Å
c = 19.6406 (6) Å
V = 5648.4 (3) Å^3
Z = 8
F(000) = 2952
D_x = 1.736 Mg m^{-3}
Mo $K\alpha$ radiation, λ = 0.71075 Å
Cell parameters from 13504 reflections
θ = 2.6–27.5°
μ = 3.56 mm^{-1}
T = 100 K
Lath, dark green
0.19 × 0.01 × 0.01 mm

Data collection

Rigaku FRE+ diffractometer equipped with HF Varimax confocal mirrors and an AFC12 goniometer and HG Saturn 724+ detector
Radiation source: Rotating Anode, Rigaku FRE+
Confocal mirrors, HF Varimax monochromator
Detector resolution: 28.5714 pixels mm^{-1}
profile data from ω–scans
Absorption correction: multi-scan (CrysAlis PRO; Rigaku OD, 2021)
T_{min} = 0.740, T_{max} = 1.000
36848 measured reflections
6477 independent reflections
4297 reflections with $I > 2\sigma(I)$
R_{int} = 0.088
θ_{max} = 27.5°, θ_{min} = 2.1°
h = −15→16
k = −30→28
l = −25→22

Refinement

Refinement on F^2
Least-squares matrix: full
$R[F^2 > 2\sigma(F^2)]$ = 0.057
$wR(F^2)$ = 0.130
S = 1.01
6477 reflections
360 parameters
6 restraints

Primary atom site location: dual
Hydrogen site location: mixed
H atoms treated by a mixture of independent and constrained refinement

$w = 1/[\sigma^2(F_o^2) + (0.0514P)^2 + 12.8609P]$ where $P = (F_o^2 + 2F_c^2)/3$
$(\Delta/\sigma)_{max} = 0.001$
$\Delta\rho_{max} = 0.68$ e Å^{-3}
$\Delta\rho_{min} = -0.78$ e Å^{-3}

Special details

Geometry. All e.s.d.'s (except the e.s.d. in the dihedral angle between two l.s. planes) are estimated using the full covariance matrix. The cell e.s.d.'s are taken into account individually in the estimation of e.s.d.'s in distances, angles and torsion angles; correlations between e.s.d.'s in cell parameters are only used when they are defined by crystal symmetry. An approximate (isotropic) treatment of cell e.s.d.'s is used for estimating e.s.d.'s involving l.s. planes.

Refinement. H-atoms bonded to N-atoms were located in the difference map and refined with the riding model. All N—H atom pairs were refined with an equal distance geometric restraint. The solvent water molecule was refined as a rigid body group.

Fractional atomic coordinates and isotropic or equivalent isotropic displacement parameters (Å²)

	x	*y*	*z*	U_{iso}*/U_{eq}
Br11	1.13632 (5)	0.95165 (3)	0.48873 (4)	0.0628 (3)
Br21	0.40926 (4)	0.48998 (2)	0.39309 (3)	0.03039 (15)
Fe1	0.73206 (5)	0.71905 (3)	0.57014 (4)	0.02070 (17)
S11	0.74079 (10)	0.63438 (5)	0.64326 (7)	0.0263 (3)
S21	0.68261 (10)	0.79079 (5)	0.65684 (7)	0.0281 (3)
O11	0.7817 (3)	0.77756 (15)	0.50614 (18)	0.0292 (8)
O21	0.7228 (3)	0.66978 (15)	0.49042 (18)	0.0283 (8)
N11	0.8946 (3)	0.72721 (17)	0.6116 (2)	0.0214 (9)
N12	0.9239 (3)	0.69112 (19)	0.6653 (2)	0.0289 (10)
H12	0.983 (3)	0.700 (2)	0.687 (2)	0.035*
N13	0.8917 (3)	0.61777 (19)	0.7379 (2)	0.0296 (10)
H13	0.955 (3)	0.623 (2)	0.757 (3)	0.035*
N21	0.5579 (3)	0.71085 (16)	0.5705 (2)	0.0201 (9)
N22	0.4980 (3)	0.74451 (18)	0.6141 (2)	0.0257 (10)
H22	0.429 (3)	0.738 (2)	0.619 (3)	0.031*
N23	0.4797 (3)	0.81161 (18)	0.6965 (2)	0.0263 (10)
H23	0.411 (3)	0.806 (2)	0.691 (3)	0.032*
C11	0.9498 (4)	0.8108 (2)	0.5479 (3)	0.0256 (11)
C12	0.8607 (4)	0.8145 (2)	0.5051 (3)	0.0244 (11)
C13	0.8551 (4)	0.8600 (2)	0.4577 (3)	0.0290 (12)
H13A	0.794568	0.862823	0.428075	0.035*
C14	0.9363 (4)	0.9000 (2)	0.4539 (3)	0.0347 (13)
H14	0.931037	0.930904	0.422416	0.042*
C15	1.0260 (4)	0.8955 (2)	0.4958 (3)	0.0338 (13)
C16	1.0352 (4)	0.8516 (2)	0.5418 (3)	0.0323 (13)
H16	1.097990	0.848317	0.569491	0.039*
C17	0.9642 (4)	0.7670 (2)	0.5979 (3)	0.0250 (11)
H17	1.029907	0.767082	0.622988	0.030*
C18	0.8578 (4)	0.6481 (2)	0.6849 (3)	0.0235 (11)
C19	0.8305 (5)	0.5714 (2)	0.7686 (3)	0.0325 (13)
H19A	0.833418	0.537044	0.738868	0.039*

H19B	0.753821	0.582947	0.773507	0.039*
C21	0.5442 (4)	0.63170 (19)	0.4908 (2)	0.0196 (10)
C22	0.6527 (4)	0.6310 (2)	0.4691 (2)	0.0240 (11)
C23	0.6846 (4)	0.5885 (2)	0.4228 (3)	0.0340 (13)
H23A	0.757209	0.587862	0.407000	0.041*
C24	0.6126 (4)	0.5476 (2)	0.3998 (3)	0.0344 (13)
H24	0.635727	0.519082	0.368365	0.041*
C25	0.5073 (4)	0.5480 (2)	0.4224 (3)	0.0247 (11)
C26	0.4721 (4)	0.5895 (2)	0.4658 (3)	0.0237 (11)
H26	0.398377	0.590122	0.479458	0.028*
C27	0.5019 (4)	0.67281 (19)	0.5378 (2)	0.0218 (11)
H27	0.426046	0.672161	0.545748	0.026*
C28	0.5462 (4)	0.7824 (2)	0.6566 (2)	0.0227 (11)
C29	0.5135 (4)	0.8538 (2)	0.7462 (3)	0.0332 (13)
H29A	0.585645	0.842911	0.764023	0.040*
H29B	0.462069	0.853351	0.784844	0.040*
C110	0.8767 (6)	0.5569 (3)	0.8375 (4)	0.062 (2)
H11A	0.952479	0.545279	0.832449	0.092*
H11B	0.835241	0.525371	0.857747	0.092*
H11C	0.872465	0.590771	0.867077	0.092*
C210	0.5192 (6)	0.9129 (3)	0.7180 (3)	0.0533 (18)
H21A	0.569115	0.913513	0.679198	0.080*
H21B	0.545244	0.939345	0.753204	0.080*
H21C	0.447095	0.924889	0.702894	0.080*
O101	0.7818 (3)	0.7444 (2)	0.3686 (2)	0.0540 (12)
H10A	0.751602	0.725563	0.336775	0.081*
H10B	0.749073	0.733786	0.404481	0.081*
O201	1.2660 (4)	0.6526 (2)	0.7620 (3)	0.0714 (15)
O202	1.1333 (4)	0.6918 (3)	0.7100 (3)	0.089 (2)
O203	1.1007 (4)	0.6406 (3)	0.7980 (2)	0.0736 (17)
N201	1.1666 (4)	0.6618 (2)	0.7581 (3)	0.0460 (13)

Atomic displacement parameters (Å²)

	U^{11}	U^{22}	U^{33}	U^{12}	U^{13}	U^{23}
Br11	0.0369 (4)	0.0510 (4)	0.1004 (6)	−0.0233 (3)	−0.0197 (4)	0.0426 (4)
Br21	0.0335 (3)	0.0198 (2)	0.0379 (3)	−0.0054 (2)	−0.0136 (3)	−0.0019 (2)
Fe1	0.0152 (3)	0.0184 (4)	0.0284 (4)	−0.0044 (3)	−0.0018 (3)	−0.0002 (3)
S11	0.0205 (6)	0.0234 (7)	0.0348 (7)	−0.0046 (5)	−0.0026 (6)	0.0014 (5)
S21	0.0193 (6)	0.0255 (7)	0.0394 (8)	−0.0027 (5)	−0.0049 (6)	−0.0095 (6)
O11	0.0213 (18)	0.038 (2)	0.028 (2)	−0.0125 (16)	−0.0058 (16)	0.0004 (16)
O21	0.0230 (19)	0.031 (2)	0.030 (2)	−0.0085 (15)	0.0049 (16)	−0.0068 (16)
N11	0.017 (2)	0.022 (2)	0.025 (2)	−0.0014 (16)	0.0023 (18)	0.0014 (17)
N12	0.022 (2)	0.030 (2)	0.035 (3)	−0.0082 (19)	−0.008 (2)	0.0061 (19)
N13	0.024 (2)	0.028 (2)	0.036 (3)	−0.0020 (19)	−0.004 (2)	0.006 (2)
N21	0.018 (2)	0.017 (2)	0.026 (2)	0.0008 (16)	−0.0008 (18)	0.0010 (16)
N22	0.018 (2)	0.026 (2)	0.033 (3)	−0.0015 (18)	0.002 (2)	−0.0062 (19)
N23	0.018 (2)	0.031 (2)	0.030 (3)	0.0014 (18)	−0.005 (2)	−0.0043 (19)

C11	0.021 (3)	0.021 (3)	0.035 (3)	0.000 (2)	0.003 (2)	0.001 (2)
C12	0.023 (3)	0.024 (3)	0.027 (3)	−0.002 (2)	0.005 (2)	−0.002 (2)
C13	0.027 (3)	0.032 (3)	0.028 (3)	−0.001 (2)	−0.006 (2)	0.003 (2)
C14	0.032 (3)	0.029 (3)	0.043 (3)	0.000 (2)	0.002 (3)	0.009 (2)
C15	0.023 (3)	0.030 (3)	0.048 (4)	−0.004 (2)	0.003 (3)	0.009 (3)
C16	0.024 (3)	0.029 (3)	0.044 (4)	−0.004 (2)	−0.005 (3)	0.008 (2)
C17	0.016 (2)	0.026 (3)	0.032 (3)	−0.004 (2)	0.000 (2)	−0.001 (2)
C18	0.026 (3)	0.019 (3)	0.026 (3)	0.001 (2)	0.004 (2)	0.001 (2)
C19	0.037 (3)	0.022 (3)	0.038 (3)	−0.004 (2)	0.004 (3)	0.004 (2)
C21	0.019 (2)	0.014 (2)	0.025 (3)	−0.0010 (18)	−0.007 (2)	0.0025 (19)
C22	0.028 (3)	0.026 (3)	0.018 (3)	−0.005 (2)	−0.004 (2)	0.000 (2)
C23	0.027 (3)	0.033 (3)	0.041 (3)	−0.006 (2)	0.002 (3)	−0.012 (3)
C24	0.037 (3)	0.028 (3)	0.038 (3)	−0.005 (2)	−0.002 (3)	−0.012 (2)
C25	0.022 (3)	0.021 (3)	0.031 (3)	−0.007 (2)	−0.012 (2)	0.003 (2)
C26	0.015 (2)	0.019 (3)	0.037 (3)	0.0011 (19)	−0.011 (2)	0.004 (2)
C27	0.015 (2)	0.020 (3)	0.031 (3)	−0.0004 (19)	−0.005 (2)	0.005 (2)
C28	0.023 (3)	0.021 (3)	0.024 (3)	0.001 (2)	−0.002 (2)	0.002 (2)
C29	0.027 (3)	0.038 (3)	0.034 (3)	0.000 (2)	−0.006 (3)	−0.010 (2)
C110	0.068 (5)	0.057 (5)	0.059 (5)	−0.025 (4)	−0.006 (4)	0.023 (4)
C210	0.058 (4)	0.046 (4)	0.056 (4)	−0.006 (3)	−0.007 (4)	−0.013 (3)
O101	0.032 (2)	0.093 (4)	0.037 (2)	−0.016 (2)	0.003 (2)	−0.006 (3)
O201	0.029 (3)	0.094 (4)	0.091 (4)	−0.005 (3)	−0.011 (3)	0.008 (3)
O202	0.029 (3)	0.147 (5)	0.091 (4)	−0.023 (3)	−0.014 (3)	0.074 (4)
O203	0.045 (3)	0.124 (5)	0.052 (3)	−0.024 (3)	0.001 (2)	0.032 (3)
N201	0.034 (3)	0.058 (4)	0.046 (3)	−0.014 (3)	−0.010 (3)	0.004 (3)

Geometric parameters (Å, º)

Br11—C15	1.894 (5)	C14—C15	1.385 (8)
Br21—C25	1.903 (5)	C15—C16	1.369 (7)
Fe1—S11	2.4404 (15)	C16—H16	0.9500
Fe1—S21	2.4615 (14)	C17—H17	0.9500
Fe1—O11	1.952 (3)	C19—H19A	0.9900
Fe1—O21	1.944 (3)	C19—H19B	0.9900
Fe1—N11	2.176 (4)	C19—C110	1.506 (8)
Fe1—N21	2.161 (4)	C21—C22	1.407 (7)
S11—C18	1.692 (5)	C21—C26	1.414 (6)
S21—C28	1.698 (5)	C21—C27	1.429 (7)
O11—C12	1.302 (6)	C22—C23	1.399 (7)
O21—C22	1.320 (6)	C23—H23A	0.9500
N11—N12	1.396 (6)	C23—C24	1.381 (7)
N11—C17	1.293 (6)	C24—H24	0.9500
N12—H12	0.87 (3)	C24—C25	1.374 (7)
N12—C18	1.349 (6)	C25—C26	1.360 (7)
N13—H13	0.88 (3)	C26—H26	0.9500
N13—C18	1.325 (6)	C27—H27	0.9500
N13—C19	1.449 (6)	C29—H29A	0.9900
N21—N22	1.376 (5)	C29—H29B	0.9900

N21—C27	1.295 (6)	C29—C210	1.486 (8)
N22—H22	0.87 (3)	C110—H11A	0.9800
N22—C28	1.352 (6)	C110—H11B	0.9800
N23—H23	0.87 (3)	C110—H11C	0.9800
N23—C28	1.322 (6)	C210—H21A	0.9800
N23—C29	1.446 (6)	C210—H21B	0.9800
C11—C12	1.388 (7)	C210—H21C	0.9800
C11—C16	1.424 (7)	O101—H10A	0.8498
C11—C17	1.426 (7)	O101—H10B	0.8487
C12—C13	1.411 (7)	O201—N201	1.249 (6)
C13—H13A	0.9500	O202—N201	1.246 (7)
C13—C14	1.372 (7)	O203—N201	1.232 (6)
C14—H14	0.9500		

S11—Fe1—S21	98.70 (5)	C11—C17—H17	117.5
O11—Fe1—S11	158.16 (11)	N12—C18—S11	121.3 (4)
O11—Fe1—S21	92.89 (11)	N13—C18—S11	123.3 (4)
O11—Fe1—N11	83.71 (14)	N13—C18—N12	115.4 (5)
O11—Fe1—N21	112.13 (14)	N13—C19—H19A	109.7
O21—Fe1—S11	90.03 (11)	N13—C19—H19B	109.7
O21—Fe1—S21	160.48 (11)	N13—C19—C110	110.0 (5)
O21—Fe1—O11	84.89 (15)	H19A—C19—H19B	108.2
O21—Fe1—N11	114.03 (15)	C110—C19—H19A	109.7
O21—Fe1—N21	83.82 (14)	C110—C19—H19B	109.7
N11—Fe1—S11	79.00 (11)	C22—C21—C26	119.2 (4)
N11—Fe1—S21	84.89 (11)	C22—C21—C27	123.5 (4)
N21—Fe1—S11	88.32 (11)	C26—C21—C27	117.3 (4)
N21—Fe1—S21	79.05 (11)	O21—C22—C21	121.5 (4)
N21—Fe1—N11	157.80 (15)	O21—C22—C23	120.3 (5)
C18—S11—Fe1	99.81 (17)	C23—C22—C21	118.2 (4)
C28—S21—Fe1	99.60 (17)	C22—C23—H23A	119.4
C12—O11—Fe1	134.9 (3)	C24—C23—C22	121.2 (5)
C22—O21—Fe1	134.2 (3)	C24—C23—H23A	119.4
N12—N11—Fe1	118.0 (3)	C23—C24—H24	120.0
C17—N11—Fe1	126.8 (3)	C25—C24—C23	120.0 (5)
C17—N11—N12	114.6 (4)	C25—C24—H24	120.0
N11—N12—H12	117 (4)	C24—C25—Br21	120.0 (4)
C18—N12—N11	120.4 (4)	C26—C25—Br21	119.3 (4)
C18—N12—H12	123 (4)	C26—C25—C24	120.7 (5)
C18—N13—H13	123 (4)	C21—C26—H26	119.7
C18—N13—C19	123.9 (4)	C25—C26—C21	120.6 (5)
C19—N13—H13	113 (4)	C25—C26—H26	119.7
N22—N21—Fe1	119.2 (3)	N21—C27—C21	125.6 (4)
C27—N21—Fe1	126.3 (3)	N21—C27—H27	117.2
C27—N21—N22	114.2 (4)	C21—C27—H27	117.2
N21—N22—H22	120 (4)	N22—C28—S21	120.9 (4)
C28—N22—N21	121.2 (4)	N23—C28—S21	123.8 (4)
C28—N22—H22	118 (4)	N23—C28—N22	115.3 (4)

C28—N23—H23	118 (4)	N23—C29—H29A	109.0
C28—N23—C29	124.7 (4)	N23—C29—H29B	109.0
C29—N23—H23	117 (4)	N23—C29—C210	112.9 (5)
C12—C11—C16	119.7 (5)	H29A—C29—H29B	107.8
C12—C11—C17	124.1 (5)	C210—C29—H29A	109.0
C16—C11—C17	116.2 (5)	C210—C29—H29B	109.0
O11—C12—C11	123.0 (5)	C19—C110—H11A	109.5
O11—C12—C13	117.9 (5)	C19—C110—H11B	109.5
C11—C12—C13	119.0 (5)	C19—C110—H11C	109.5
C12—C13—H13A	119.7	H11A—C110—H11B	109.5
C14—C13—C12	120.6 (5)	H11A—C110—H11C	109.5
C14—C13—H13A	119.7	H11B—C110—H11C	109.5
C13—C14—H14	120.0	C29—C210—H21A	109.5
C13—C14—C15	120.1 (5)	C29—C210—H21B	109.5
C15—C14—H14	120.0	C29—C210—H21C	109.5
C14—C15—Br11	118.7 (4)	H21A—C210—H21B	109.5
C16—C15—Br11	120.3 (4)	H21A—C210—H21C	109.5
C16—C15—C14	121.1 (5)	H21B—C210—H21C	109.5
C11—C16—H16	120.3	H10A—O101—H10B	104.6
C15—C16—C11	119.4 (5)	O202—N201—O201	117.9 (5)
C15—C16—H16	120.3	O203—N201—O201	122.9 (6)
N11—C17—C11	124.9 (5)	O203—N201—O202	119.2 (5)
N11—C17—H17	117.5		

Br11—C15—C16—C11	178.1 (4)	C14—C15—C16—C11	−1.7 (9)
Br21—C25—C26—C21	177.3 (3)	C16—C11—C12—O11	177.5 (5)
Fe1—S11—C18—N12	−9.9 (4)	C16—C11—C12—C13	−1.9 (7)
Fe1—S11—C18—N13	170.6 (4)	C16—C11—C17—N11	178.4 (5)
Fe1—S21—C28—N22	−1.4 (4)	C17—N11—N12—C18	179.7 (4)
Fe1—S21—C28—N23	179.1 (4)	C17—C11—C12—O11	−0.9 (8)
Fe1—O11—C12—C11	16.4 (8)	C17—C11—C12—C13	179.7 (5)
Fe1—O11—C12—C13	−164.2 (4)	C17—C11—C16—C15	−178.7 (5)
Fe1—O21—C22—C21	23.7 (7)	C18—N13—C19—C110	−165.0 (5)
Fe1—O21—C22—C23	−157.4 (4)	C19—N13—C18—S11	−3.1 (7)
Fe1—N11—N12—C18	7.9 (6)	C19—N13—C18—N12	177.3 (5)
Fe1—N11—C17—C11	−5.6 (7)	C21—C22—C23—C24	−1.1 (8)
Fe1—N21—N22—C28	−0.2 (6)	C22—C21—C26—C25	1.3 (7)
Fe1—N21—C27—C21	−5.3 (7)	C22—C21—C27—N21	−6.3 (8)
O11—C12—C13—C14	−179.6 (5)	C22—C23—C24—C25	−0.1 (9)
O21—C22—C23—C24	180.0 (5)	C23—C24—C25—Br21	−177.9 (4)
N11—N12—C18—S11	2.8 (7)	C23—C24—C25—C26	2.0 (8)
N11—N12—C18—N13	−177.6 (4)	C24—C25—C26—C21	−2.6 (7)
N12—N11—C17—C11	−176.5 (5)	C26—C21—C22—O21	179.4 (4)
N21—N22—C28—S21	1.2 (6)	C26—C21—C22—C23	0.5 (7)
N21—N22—C28—N23	−179.2 (4)	C26—C21—C27—N21	173.1 (4)
N22—N21—C27—C21	−178.5 (4)	C27—N21—N22—C28	173.6 (4)
C11—C12—C13—C14	−0.2 (8)	C27—C21—C22—O21	−1.2 (7)
C12—C11—C16—C15	2.8 (8)	C27—C21—C22—C23	179.9 (5)

C12—C11—C17—N11	−3.2 (8)	C27—C21—C26—C25	−178.1 (4)
C12—C13—C14—C15	1.3 (8)	C28—N23—C29—C210	90.3 (6)
C13—C14—C15—Br11	179.8 (4)	C29—N23—C28—S21	−1.2 (7)
C13—C14—C15—C16	−0.4 (9)	C29—N23—C28—N22	179.3 (5)

Hydrogen-bond geometry (Å, º)

D—H···*A*	*D*—H	H···*A*	*D*···*A*	*D*—H···*A*
N12—H12···O202	0.87 (3)	1.92 (4)	2.733 (6)	155 (5)
N13—H13···O203	0.88 (3)	2.02 (3)	2.890 (6)	176 (5)
N22—H22···O101^{i}	0.87 (3)	1.85 (3)	2.695 (6)	166 (5)
N23—H23···O201^{ii}	0.87 (3)	2.23 (4)	2.887 (6)	133 (4)
O101—H10*A*···O202^{i}	0.85	1.90	2.692 (6)	155
O101—H10*B*···O11	0.85	2.28	2.809 (6)	121

Symmetry codes: (i) *x*−1/2, *y*, −*z*+1; (ii) *x*−1, −*y*+3/2, −*z*+3/2.